Wave Propagation into Complex Coastal Systems and the Role of Nonlinear Interactions

Jacco Groeneweg[1]; Marcel van Gent[2]; Joana van Nieuwkoop[3]; and Yaron Toledo[4]

Abstract: The phase-averaged wave model Simulating WAves Nearshore (SWAN) is often used for the design of dikes and harbors. However, various hindcast studies have shown that SWAN underpredicts the wave energy when waves are penetrating into bathymetries with shallow areas traversed by channels, such as tidal inlets or harbor entrances. The underprediction of these waves could lead to dike failure or shipping downtime as a consequence of incorrect hydraulic loads. This paper presents an explanation for the underprediction of this wave penetration. By comparing a series of SWAN computations with laboratory measurements and computations with the Boussinesq-type wave model TRITON, it is demonstrated that the absence of various subharmonic and superharmonic interactions in SWAN causes an unrealistic amount of energy to be trapped on the channel slopes owing to wave refraction. The two-dimensional nonlinear interactions, which appear to be present in the measurements and TRITON results, broaden the directional range of the energy density spectrum when waves propagate over a sloping bottom. Owing to the directional broadening of the spectrum, more energy exists at angles smaller than the frequency-dependent critical angle for refraction, and therefore more wave energy is transmitted into and across channels, especially when waves approach the channel under an angle. It is recommended that this insight be used to find an alternative formulation for the present one-dimensional three-wave interaction formulation in SWAN. **DOI:** **10.1061/(ASCE)WW.1943-5460.0000300.**

Author keywords: Wave modeling; Nonlinear wave interactions; Physical model tests; SWAN; Boussinesq-type.

Introduction

The prediction of wave climate under storm conditions is challenging in coastal systems with complex bathymetries such as the Wadden Sea in the Netherlands. The phase-averaged wave model Simulating WAves Nearshore (SWAN) (Booij et al. 1999) is one of the most suitable models for these large and shallow areas. Over the last couple of years, significant SWAN model improvements have been made; see e.g., Van der Westhuysen et al. (2012) and Zijlema et al. (2012). As addressed in Van der Westhuysen et al. (2012), one of the remaining issues is that SWAN underestimates the penetration of North Sea swell waves in the range of 0.03–0.20 Hz during storm conditions. This was observed in hindcasts of the Eastern Scheldt and the Dutch part of the Eastern Wadden Sea, and is illustrated in Fig. 1. Fig. 1(a) shows the bathymetry of the Eastern Wadden Sea, located in the northern part of the Netherlands, including the measurement locations WEO1, offshore of the barrier islands, and PBW1 and UHW1, near the mainland. In Figs. 1(b–d), the variance density spectra have been presented for these three locations, as well as the directional spreading as function of frequency at the most seaward location, WEO1, in Fig. 1(b), all at the peak of the storm of November 9, 2007. The wind, at the instant considered, is coming from the northwest (327°N). The offshore peak period is 13 s and the directional spreading approximately 20° at the peak frequency, and even more at higher frequencies. Between the mainland and the barrier islands, locally generated wave energy dominates the swell-wave energy penetrating from the North Sea. The peak period reduces to approximately 5 s. The measured and SWAN-computed locally generated wave energy compares very well. However, SWAN underestimates the swell-wave energy significantly at the nearshore measurement locations.

Underestimation of the swell-wave energy leads to computed levels of hydraulic loads that will be generally smaller than the measured hydraulic loads. As a consequence, the safety assessment of primary water defenses leads to incorrect conclusions if no further measures are taken. Therefore, insight into the mechanisms causing the models underestimation should be gained to improve the SWAN model, or if that is not possible, to take the right measures to deal with the obtained underestimations.

Analysis of the North Sea wave penetration into the Dutch Eastern Wadden Sea (Alkyon 2009) has shown that the underestimation of swell-wave energy near the mainland coast decreases if diagnostic modeling measures are taken. Examples of these measures are decreasing bottom friction, limiting refraction of the swell waves, applying quadratic frequency-dependent wave breaking, and/or increasing the water level. These measures are called diagnostic because they are not always physically correct and are actually meant to counteract the underestimation of swell waves due to inaccurate modeling. Alkyon (2009) also found that applying a smoothed bathymetry did not lead to a significantly higher amount of swell-wave energy near the mainland dikes, which suggests that refraction on large bathymetric gradients and/or diffraction are not a cause for the swell-wave underestimation. However, they could not positively verify the effect of diffraction on the basis of SWAN simulations only. The SWAN equations are based on the wave action transport equations, in which derivation of the eikonal part,

[1]Dept. of Coastal Structures & Waves, Deltares, P.O. Box 177, 2600 MH Delft, Netherlands (corresponding author). E-mail: Jacco.Groeneweg@Deltares.nl

[2]Dept. of Coastal Structures & Waves, Deltares, P.O. Box 177, 2600 MH Delft, Netherlands. E-mail: Marcel.vanGent@Deltares.nl

[3]Dept. of Coastal Structures & Waves, Deltares, P.O. Box 177, 2600 MH Delft, Netherlands. E-mail: Joana.vanNieuwkoop@Deltares.nl

[4]School of Mechanical Engineering, Tel-Aviv Univ., P.O. Box 39040, Tel Aviv 6997801, Israel. E-mail: Toledo@tau.ac.il

Note. This manuscript was submitted on September 2, 2014; approved on January 12, 2015; published online on April 25, 2015. Discussion period open until September 25, 2015; separate discussions must be submitted for individual papers. This paper is part of the ***Journal of Waterway, Port, Coastal, and Ocean Engineering***, © ASCE, ISSN 0733-950X/04015003(17)/$25.00.

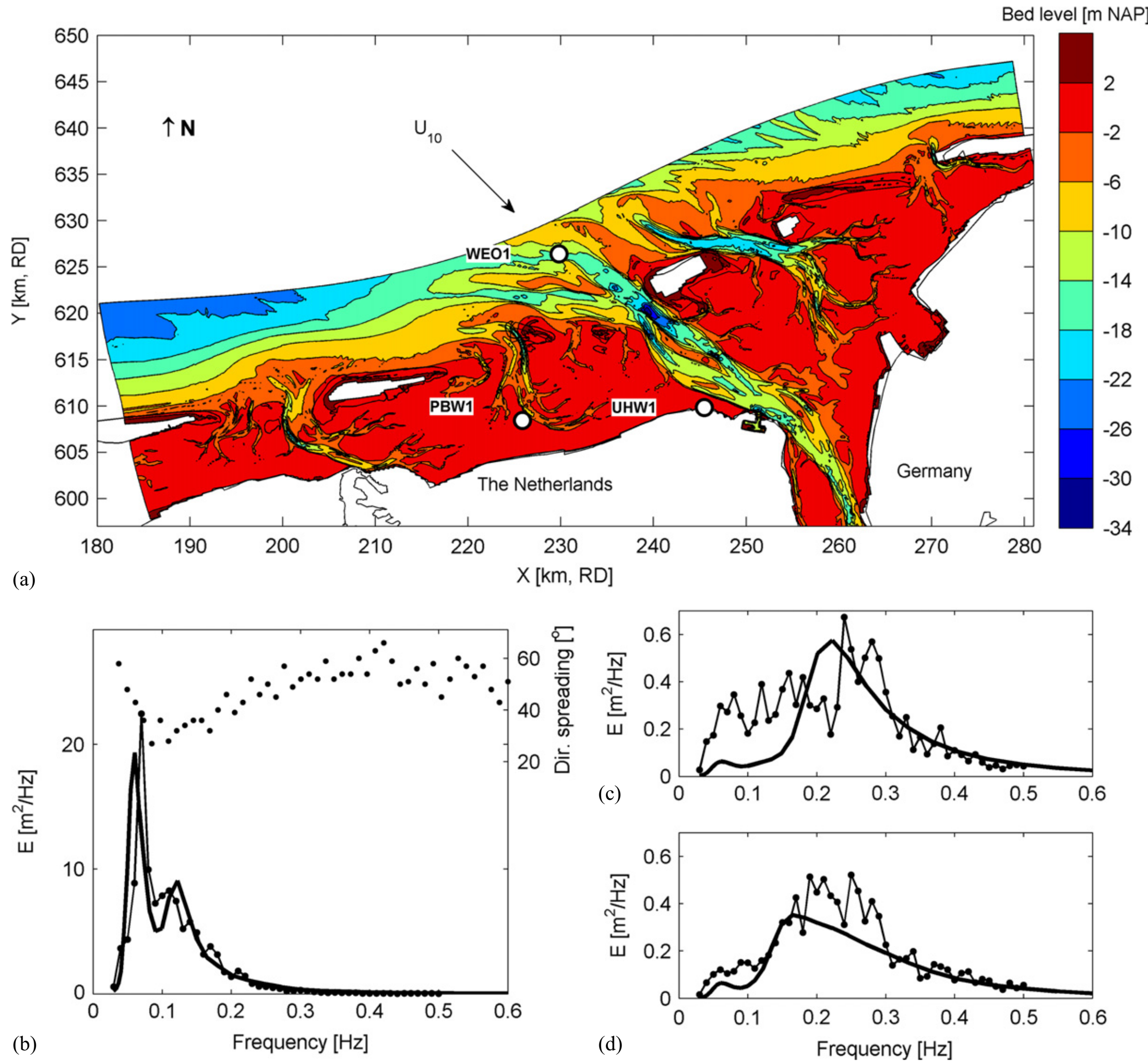

Fig. 1. (Color) Locations have been indicated in (a); bottom height in the Eastern Wadden Sea and energy density spectra at (b) WEO1; (c) PBW1; and (d) UHW1; dotted solid lines in the lower panels indicate measured variance density; the solid lines indicate the SWAN result; measured directional spreading at (b) WEO1 is indicated with dots

which governs diffraction, is neglected. The SWAN model only includes a phase-decoupled diffraction option (Holthuijsen et al. 2003), with which diffraction is modeled in an approximate way.

To identify the effect of diffraction on swell waves, Deltares and Alkyon (2009) compared results from the spectral wave model SWAN and the model PHAROS. The latter is based on the mild-slope equations and does include diffraction. The effect of diffraction was found to be local and has a negligible effect on the amount of energy that penetrates. This finding eliminates one uncertainty in SWAN with respect to the necessary modeled physics (i.e., wave diffraction) for the purpose of safety assessment in the Wadden Sea, but does not give an explanation for the reported underestimation of the swell components.

In addition, laboratory experiments were conducted by Eslami et al. (2012) to test the hypothesis that SWAN overestimates the refraction of the relatively long wave components when propagating from the deeper channel to the shallow flats. It was expected that the energy computed by SWAN would dissipate on the tidal flats before reaching the mainland. However, the laboratory experiments and successive computations with SWAN and the Boussinesq-type model TRITON (Borsboom et al. 2000) did not lead to the confirmation of this hypothesis.

Dusseljee et al. (2012) presented an intercomparison study of a SWAN model and three-dimensional (3D) laboratory experiments (performed by Deltares from Delft, Netherlands) on waves approaching and partly crossing a navigation channel towards a harbor. It was observed that SWAN underestimates the wave energy both in the channel and at the lee side of the channel for long waves propagating under a small angle with respect to the channel axis. The strong modeled wave energy reduction across the channel is in line with the conclusion in Magne et al. (2007), who studied the evolution of waves over the Scripps Canyon near San Diego, California, and concluded that swell-wave components cannot cross the canyon in the geometrical optics approximation. In the SWAN results, a large amount of wave energy is trapped on the channel slope because of wave refraction. However, as will be shown in the next section, the measured wave energy into the laboratory experiments shows that more wave energy propagates into and across the channel than was observed in the SWAN results.

When waves propagate over intermediate or shallow water depths, a different governing mechanism of energy transfer between the spectral components becomes effective. This nonlinear mechanism is governed by the closure of Bragg-type resonant conditions between wave triads and a bottom component (see e.g., Liu and Yue 1998; Alam et al. 2010; Toledo and Agnon 2009). Wave energy can be transferred through superharmonic interactions between two waves to a higher harmonic with a frequency given by the sum of the frequencies. The wave direction is determined by the sum of the wavenumber vectors of the two originating waves together with a bottom component that closes the resonance condition. In the same manner, energy can be transferred via the subharmonic interaction mechanism to lower harmonics with wave frequencies given by the differences between combinations of two waves.

Using an oblique nonlinear parabolic equation, Toledo (2013) investigated the simple case of two similar monochromatic waves propagating in mirroring attack angles (with respect to the normal of the depth contours) toward a sloping beach with no lateral changes. In the linear situation, the wave components reduce their attack angles in the refraction process. For the nonlinear situation, it was shown that the shoaling process of the primary components transfers energy via a nonlinear superharmonic self-interaction to its double-harmonic component, propagating under a smaller angle than the primary component. Via a nonlinear subharmonic interaction of this wave with the oppositely angled primary wave component, a first-harmonic wave is created. However, the propagation angle of this component is much larger than the angle of the primary component, in the example of Toledo (2013, Fig. 7) almost a factor two. From this simplified problem, it was concluded that the directional range was broadened by nonlinear shoaling. Such a nonlinear spectral broadening may result in wave components that approach the channel at larger angles with respect to the channel axis and are capable of penetrating into the channel.

In addition to investigating possible mechanisms that explain the observed mismatch between the SWAN model and field measurements in the Wadden Sea, the present study also aims to provide engineers with a way to evaluate related cases where SWAN's physical formulations may fail. Therefore, the objectives of this study are threefold. First, it aims to describe a mechanism that explains the discrepancy between modeled (SWAN) and measured wave energy in complex areas. Second, it aims to demonstrate that the nonlinear shoaling mechanism directionally broadens the wave spectrum. Third, it aims at providing engineers with a way to evaluate related cases where SWAN's physical formulations may fail.

To meet the objectives of this study, the outline of the paper is as follows. Wave basin experiments were conducted for the purpose of understanding the physical mechanism of wave penetration into and across channels (see the next section). To investigate the accuracy of SWAN, numerical runs were conducted for a simplified channel bathymetry, using TRITON as benchmark (section titled "Analysis of Simulations on Idealized Channel Geometries"). To show that the observations in the laboratory experiment can also apply to the Wadden Sea, results of SWAN computations in that region have been analyzed (section titled "Towards Practical Situations"). The study is concluded in the last section.

Laboratory Channel Experiments

Setup of Laboratory Experiments

The laboratory experiments presented in this section were performed as an additional part of 3D breakwater stability tests reported in Dusseljee et al. (2012) in the Delta Basin of Deltares, where the entrance of a port was modeled. The setup of the original tests comprised part of the foreshore and entrance channel of the port, and the two breakwater roundheads with adjacent trunk sections. The model was constructed at a scale of approximately 1:60. Details of this setup are also described by Dusseljee et al. (2012).

In the supplementary test series, six tests were performed without the two breakwaters. The layout of the model, as placed in the basin, is shown in Fig. 2. The range of the y-axis, starting at $y = 24$ m, indicates that half of the basin was used. The multidirectional wave generator is located at the left boundary ($x = 0$ m). The wave generator is equipped with active reflection compensation. This means that the motion of the wave board compensates for the waves reflected by the model preventing them from rereflecting at the wave board and propagating towards the model. The wave board is also equipped with second-order wave steering. This means that second-order effects of the first higher and first lower harmonics of the wave field are taken into account in the wave board motion, which ensures that the generated waves resemble waves that occur in nature. The upper ($y = 40$ m) and lower ($y = 24$ m) sides consist of vertical walls, and at the right boundary a sloping beach damps out most of the wave energy. In the channel

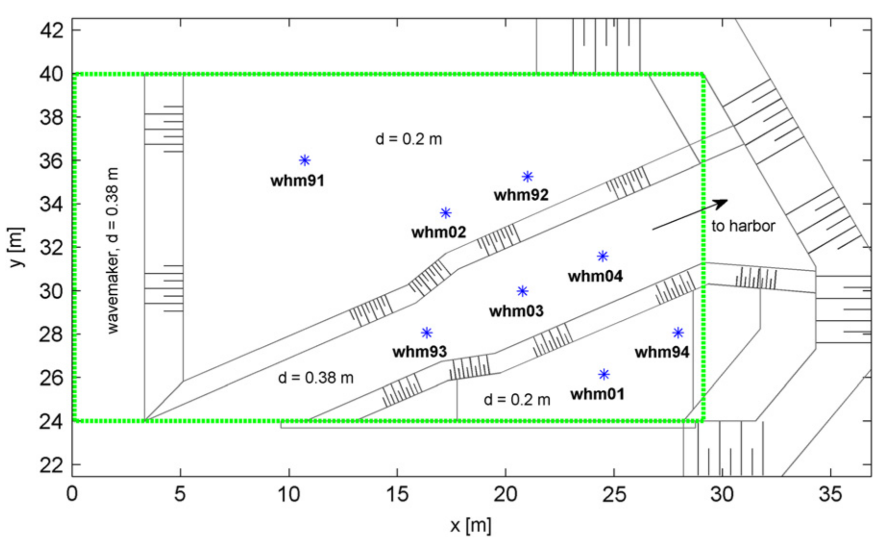

Fig. 2. (Color) Layout of the physical model, including the locations of the wave gauges; green dotted line indicates the area of the computational domain; wave gauges marked with whm0x indicate resistance-type wave gauges, whereas ones marked with whm9x indicate directional wave gauges

as well as in front of the wave generator, the water depth is 0.38 m. At a distance of 5 m from the wave generator, the water depth decreases to 0.20 m over a 1:10 transitional slope. On both sides of the channel this water depth is 0.20 m. The angle between the channel axis and the wave paddles is 65°, whereas the side slopes of the channel are 1:5. As shown in Fig. 2, at the halfway mark, the channel becomes broader.

Waves were generated with a mean direction of 90° with respect to the wave generator. A JOint North Sea WAve Project (JONSWAP) spectrum was applied. Three values of the peak wave period (1.23, 1.45, 1.87 s) and two values of the directional spreading (normal distribution with $\sigma = 0°$ or $\sigma = 20°$) define the test matrix of six test cases. The significant wave height is 0.082 m in all test cases. The six test cases have been defined in Table 1. Given the scale of 1:60, the wave parameter values in Table 1 represent the offshore North Sea wave climate under typical storm conditions. The value of 20° directional spreading is a realistic value for waves at the North Sea, as is also illustrated in Fig. 1(b). At station WEO1, offshore of the barrier islands, a directional spreading has been measured at the peak frequency of slightly more than 20°. Inside the Wadden Sea, the directional spreading is larger (not shown).

Waves were measured at eight locations, both in the channel and on either side of the channel, by using four standard resistance-type wave gauges (whm01, whm02, whm03, whm04 in Fig. 2) and four GRSM directional wave gauges (whm91, whm92, whm93, whm94). A GRSM measures the surface elevation and the two-dimensional (2D) horizontal wave orbital velocities. These time series have been processed into a 2D directional variance spectrum using the maximum entropy method (see Kobune and Hashimoto 1986). This method was shown to provide high-standard directional wave information obtained from point sources such as directional wave gauges or directional wave buoys [see e.g., Benoit et al. (1997) and Kim et al. (1994)].

SWAN and TRITON Model Setup

Both a SWAN and a TRITON model were set up for the laboratory experiment. The SWAN model computed the propagation and transformation of directional wave-action density spectra. The geographical resolution in both directions was 10 cm, which was fine enough to resolve the variation in wave energy and properly represent the bottom variations of the transitional slope and channel slopes. The full directional circle was resolved with 1.5° directional bin. For all cases, a frequency range of 0.2–3 Hz was considered, where the frequencies were distributed logarithmically.

The computations were performed using the SWAN model version 40.72ABCDE in stationary third-generation mode. The physical settings were similar to those in Van der Westhuysen et al. (2012), noting that the deepwater physics in terms of wind generation, whitecapping, and nonlinear four-wave interactions were switched off. The shallow water source terms included triad nonlinear interaction according to Eldeberky (1996) through the so-called lumped triad approximation (LTA) with $\alpha_{EB} = 0.10$ and $f_{\max,EB} = 2.5 f_{m01}$ (high-frequency cutoff for the non-linear transfer). The bottom friction was modeled according to Hasselmann et al. (1973) with the coefficient $C_{f,\mathrm{JON}} = 0.038\ \mathrm{m^2/s^3}$. For depth-induced breaking, the biphase breaker model of Van der Westhuysen (2010) was applied, with the extension proposed by Van der Westhuysen (2009). The convergence criteria applied are the so-called curvature-based criteria proposed by Zijlema and Van der Westhuysen (2005).

The TRITON model is a Boussinesq-type wave model that was developed by Borsboom et al. (2000). It simulates, up to a certain accuracy, related to a specific depth range, the full wave dynamics. This includes all wave processes such as dispersion, diffraction, refraction, shoaling, and nonlinear wave–wave interaction. Dissipative processes such as bottom friction and wave breaking are modeled by parameterizations (see Groeneweg et al. 2002). Because TRITON is a phase-resolving model, full information on wave height, phase, and direction is available. This comes at a cost; simulations by TRITON take large computational times compared with SWAN. To represent the primary waves and the higher-order harmonics properly, the TRITON simulations have been carried out on a fine grid with a resolution of 0.025 m in the x-direction, i.e., the mean-wave direction, and 0.05 m in the y-direction. The time step is 0.025 s, which is required to fulfill the CFL criterion.

At the inflow boundary JONSWAP spectra, defined by the integral wave parameters given in Table 1, are imposed. The TRITON model converts the spectra into time series of surface elevations, which are imposed in combination with a radiative condition that absorbs the rereflected waves. At the outflow boundary, a radiative boundary condition is imposed, absorbing the outgoing waves to an optimal extent. Details on the formulation of the boundary conditions are given in Borsboom et al. (2000). In SWAN, no boundary conditions need to be imposed at the outflow boundary. In both SWAN and TRITON, the lateral boundaries are modeled as fully reflective boundaries, representing the vertical walls in the laboratory tests. More specifically, in TRITON the lateral boundaries are closed and therefore fully reflect all waves attacking the lateral walls. The lateral boundaries in the SWAN model are included as fully reflective obstacles.

All TRITON computations run for 1,800 s. As a result, time series of the surface elevation and the two horizontal wave computations are obtained. To compare with the spectral wave parameters that SWAN produces, the one-dimensional (1D) and 2D spectra as well as integral wave parameters have been derived from the TRITON time series of the surface elevation and velocity components.

Comparison of Model Results with Measured Laboratory Data

For all cases mentioned in Table 1, both SWAN and TRITON computations were made. At the measurement locations measured and computed variance density spectra have been determined. In Fig. 3, the computed and measured 1D variance density spectra, as well as the resulting significant wave heights for Test T002, have been given. In Fig. 4, the measured and computed 2D variance density spectra at the locations of the four directional wave gauges have been presented.

At the three locations at the upwave side of the channel (whm91, whm02, whm92), the 1D energy density spectra are comparable. Wave breaking on the transition slope is limited. Only the most energetic waves break. The SWAN model slightly overpredicts the energy of the second harmonics. The difference between measured and SWAN-computed and TRITON-computed significant wave heights is less than 10% at all three locations.

Table 1. Test Program of the Laboratory Experiments

Name	H_{m0} (m)	T_p (s)	Dir. spr. (degrees)
T001	0.082	1.87	0
T002	0.082	1.87	20
T003	0.082	1.45	0
T004	0.082	1.45	20
T005	0.082	1.23	0
T006	0.082	1.23	20

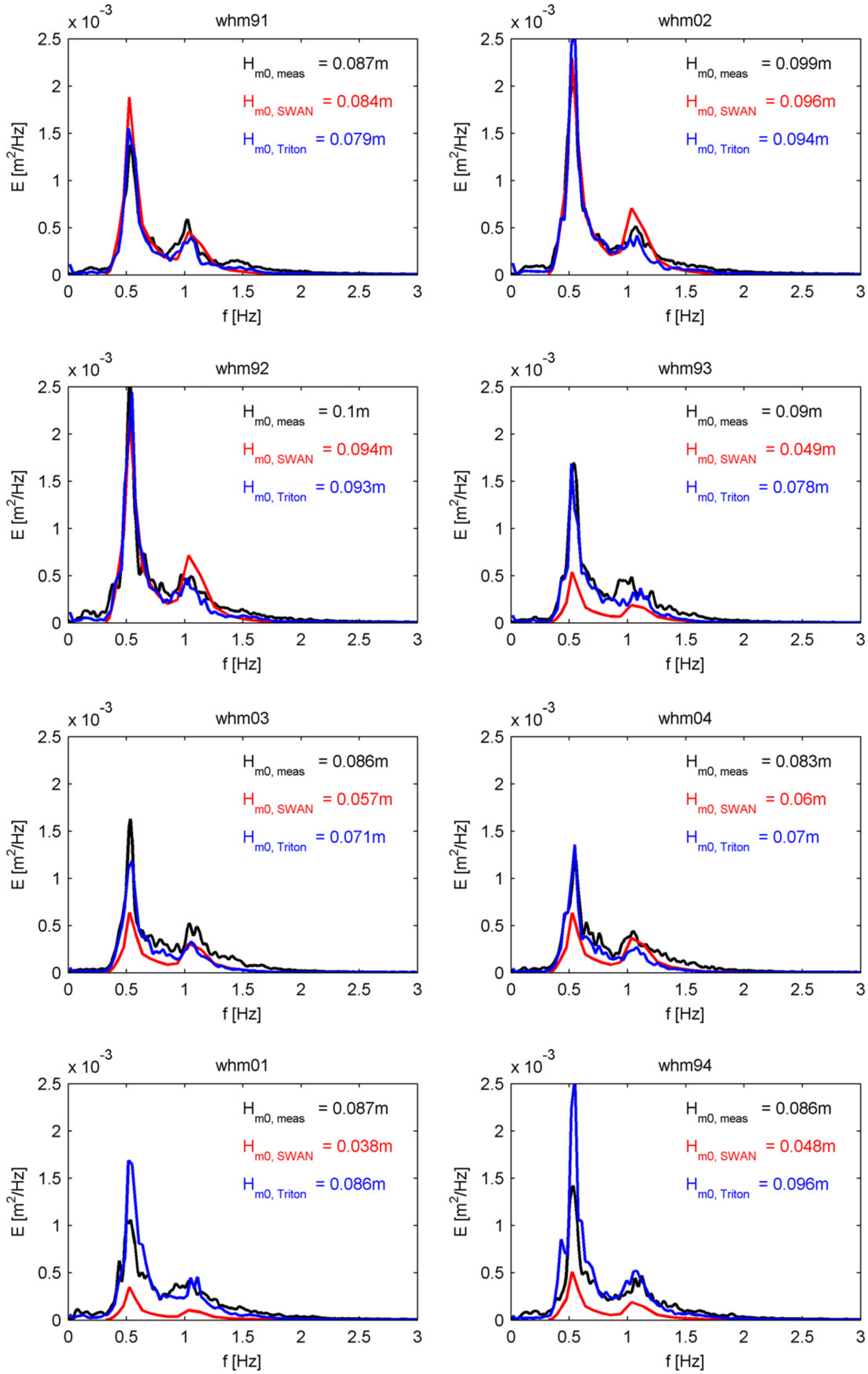

Fig. 3. (Color) Measured (black line) and computed (SWAN, red and TRITON, blue) 1D variance densities for Test T002 ($H_{m0} = 0.082$ m, $T_p = 1.87$ s, Dir. spr. = 20°) at the eight measurement locations

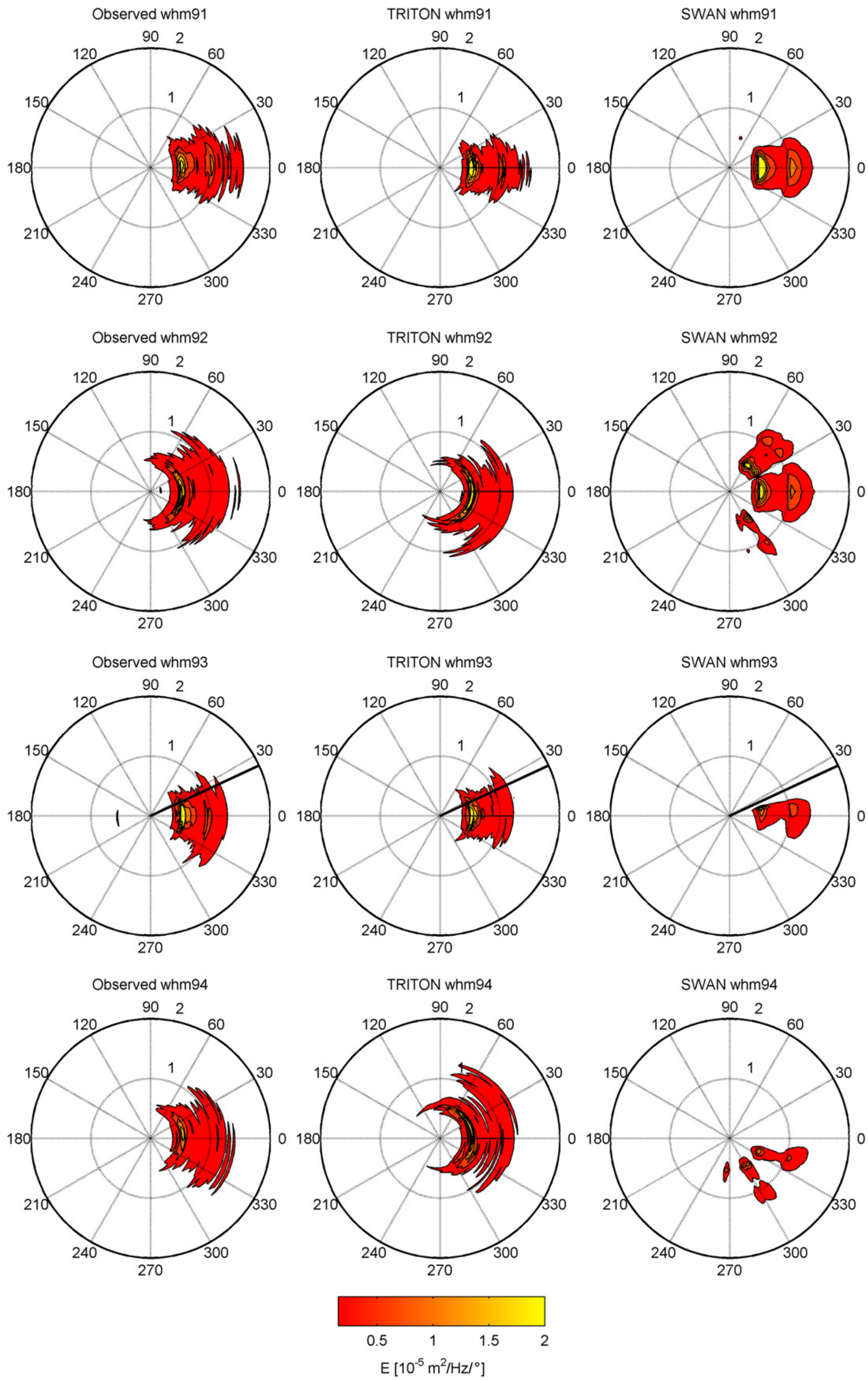

Fig. 4. (Color) Two-dimensional variance densities (observed, TRITON, and SWAN) for Test T002 at the four directional wave gauge locations (Cartesian convention); in the spectra at whm93, the solid black line indicates the channel axis; directional measurements expose significant qualitative differences between the results of the two models; TRITON's results grasp much better the directional spreading of the wave spectra

Inside the channel, the behavior at the three measurement locations (whm93, whm03, whm04) is similar. The energy level at the primary peak as produced by TRITON agrees well with the observations. The energy at the secondary peak is slightly underpredicted by TRITON. This is due to the fact that the assumption in TRITON, i.e., that higher-order nonlinear terms of order $\varepsilon\mu^2$ can be neglected, is slightly violated. Here ε and μ indicate the relative importance of nonlinear effects and dispersion, respectively. As a consequence, TRITON underestimates the significant wave height inside the channel by approximately 15%. At the three channel locations, SWAN shows a similar underestimation of the energy at the second peak. However, the energy at the primary peak is significantly smaller compared with the measurements. Consequently, the underestimation of the wave height by SWAN is larger than by TRITON, i.e., approximately 30–45%. The underprediction by SWAN is also observed downwave of the channel (whm01, whm94). At these locations TRITON overpredicts the energy at the primary peak. This is caused by the radiative boundary condition in TRITON that fully absorbs the energy from the mean wave direction, but partly reflects energy from the other directions.

The directional wave gauges in Fig. 4 show that the variance density spectrum broadens in directional space over the shallow flat from whm91 to whm92. This broadening of the spectrum at location whm92 is caused by wave reflection from the side wall and the channel. Note that for all spectra, the variance density above a certain threshold has been shown. In Fig. 4, the threshold is $0.2 \cdot 10^{-5}$ m^2/Hz/degree. The computed spectra by TRITON and the measured spectra in the shallow region (whm91 and whm92) are comparable. The SWAN model shows two main parts in the variance density spectrum. One represents the energy directly propagating from offshore. The second one propagating under an angle of approximately 45° is caused by refraction from the channel. An additional peak with a peak direction of 310° occurs owing to reflections from the side wall.

In the variance density spectra at the channel Location whm93, the channel axis is indicated by the solid line at 25°. The measured and TRITON-computed variance density spectra at whm93 are comparable. The model SWAN, on the other hand, predicts no wave energy for wave components propagating under a sharp angle with the channel axis. Refraction hampers the energy from getting into the channel. As a consequence, the energy across the channel (whm94) is strongly underpredicted by SWAN. The SWAN model's underprediction is further illustrated by integrating the energy over the directional range (15°, 35°), i.e., the range of wave components that propagate from Location whm93 and are able to reach the harbor entrance. Fig. 5 clearly shows that TRITON resembles the sectorial measured energy density spectrum $E_{\Delta d}$ rather well, whereas SWAN strongly underpredicts the energy in this relevant directional sector.

The strong reduction of the energy level at the primary peak by SWAN is observed in all test cases, whereas the TRITON spectra resemble the measured spectra well. To further illustrate the differences between the TRITON and SWAN results, the spatial distribution of the significant wave height for Test T002 has been presented in Fig. 6. The black lines indicate the channel slopes as well as the transition slope. In the wave height distribution of SWAN [Fig. 6(a)], three areas can be clearly distinguished: (1) the shallow area, where the wave height is 0.08–0.10 m; (2) the channel and the downwave side of the channel, where the wave height is 0.06–0.07 m; and (3) the upper edge at the upwave side of the channel, where the wave height increases up to 0.12 m.

The SWAN computations show that a large part of the wave energy is accumulated along the channel edge. Refraction hampers the energy from entering the channel. From Snell's law, the critical angle with respect to the channel slope normal for Test T002 is 49°, based on the peak period of 1.87 s and peak wave direction of 0°. In other words, a monochromatic wave approaching the channel under an angle of 65° with respect to channel slope normal would not be able to enter the channel owing to wave refraction on the channel slope.

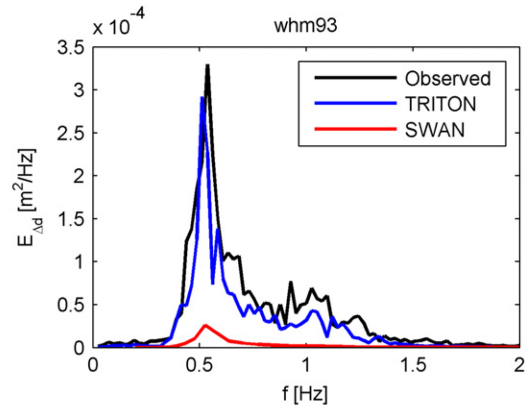

Fig. 5. (Color) Variance densities (observed, TRITON, and SWAN) for Test T002, integrated over the directional sector 15–35°; sectorial wave energy integration reveals SWAN's lack of capability to accurately predict the wave-energy propagation towards the harbor

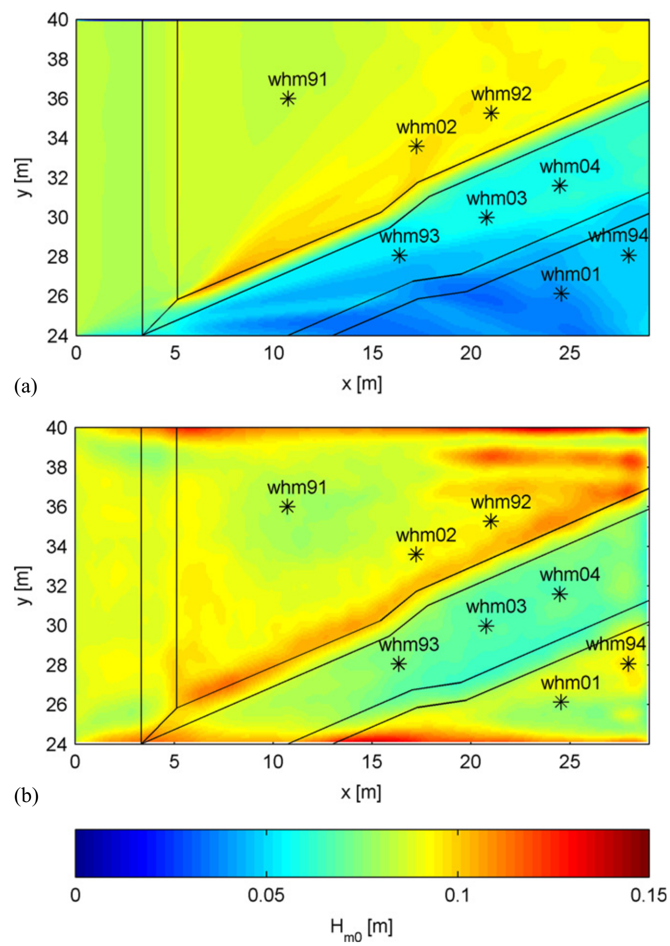

Fig. 6. (Color) Significant wave height computed by (a) SWAN and (b) TRITON for Test T002

At the upwave side of the channel, TRITON shows similar behavior as SWAN from a qualitative point of view [Fig. 6(b)]. The TRITON model predicts more energy at the closed side walls owing to reflection. Also, at the channel edge, the significant wave height is slightly larger than predicted by SWAN. The TRITON model includes reflection of wave energy at the channel edge. In the upper left corner of the domain, streaks of increased wave height also indicate partial reflection at the outflow boundary. Most interesting is the fact that TRITON predicts more wave energy in and across the channel than does SWAN.

Analysis of Simulations on Idealized Channel Geometries

In the previous section, clear differences were observed in the results of SWAN compared with TRITON in and across the channel. Diffraction, which was not activated in SWAN, might be suggested as a possible contributor to channel penetration by waves. However, a typical snapshot of the TRITON surface-elevation field (not presented here) shows some turning of the wave crests but not the radial propagation one would expect from diffraction. Furthermore, reflections on the upwave side of the channel edge due to the changes in bed level are not modeled in SWAN. However, this mechanism would rather exaggerate than reduce the accumulation of energy in this area.

Another mechanism causing the waves to propagate into the channel is nonlinear wave interactions. To verify the effect of nonlinear interactions, the channel test from the section "Laboratory Channel Experiments" has been simplified. The bend in the channel slope has been removed. Furthermore, the slope at the downwave side of the channel has been removed. This results in a bathymetry with the same transitional slope as the original bathymetry, followed by a shallow and a deep part with a 1:5 slope under a 65° angle with respect to the offshore boundary at $x = 0$. The simplified bathymetry has been presented in Fig. 7, including four output locations at the shallow and deep regions of the model setup.

For this more idealized situation, both SWAN and TRITON computations were made for the Tests T003 and T004 of Table 1 ($T_p = 1.45$ s. Results of both directionally narrow- and broad-banded tests are discussed here. To investigate the effect of the attack angle, the channel axis has been varied to directions of 30°, 50°, and 75°, in comparison with the presently considered 65°.

Directionally Narrow-Banded Waves over an Idealized Bathymetry

First, results of the directionally narrow-banded test, T003, are presented. This test is of interest because the effect of refraction is highlighted for a directionally narrow-banded wave field. To investigate the effect of nonlinear wave interactions, the results of the original nonlinear case were compared with those of the linear case, with a significant wave height of 0.00082 m, i.e., a factor of 100 smaller than the original wave height. The other wave parameters remained the same.

In Fig. 8, normalized variance density spectra are presented, obtained by TRITON (left column) and by SWAN (right column), at the shallow Location B and the deep Location D (indicated in Fig. 7) for nonlinear and linear wave spectra input. This leads to eight variance density spectra. To compare the variance densities of the linear and nonlinear inputs, the variance densities are normalized with the total variance at Location A, i.e., upwave of the transitional slope. The SWAN model's spectra at Location D in the linear [Fig. 8(d)] and nonlinear [Fig. 8(h)] cases show a similar amount of directional spreading. Because of the transfer of energy to the second harmonic at the transitional slope, more second-harmonic energy is present in the nonlinear case compared with the linear case. After penetrating into the channel (Location D), the energy at the primary peak is present neither in the linear nor in the nonlinear cases, as further illustrated in the frequency spectra in Fig. 9 (red lines). This is because refraction hampers these wave components from entering the channel. In contrast with the peak frequency waves, components of frequencies larger than 1 Hz are less affected by the bottom slope and are not refracted at the channel slope.

TRITON's results present a different behavior. First, already in the shallow region (Location B), TRITON's spectra have a broader directional spreading than the spreading seen in SWAN's. Both in the linear and nonlinear inputs, the linear diffraction mechanism diffuses wave energy. The stronger the gradients in the wave fields, the more predominant the mechanism of diffraction will be. The directional spreading in the TRITON spectra is particularly large at the primary peak. Consequently, compared with SWAN, more wave components approach the channel at an angle smaller, compared with the channel slope normal, than the critical angle, and are able to propagate into the channel. For this reason, energy at the primary peak is observed at Location D in both the linear and nonlinear cases. This is further illustrated in Fig. 9, which also shows the strong difference with SWAN's 1D spectra. From Figs. 8(a and e), it can be seen that the directional spreading at Location B is comparable, when comparing the linear and nonlinear TRITON results. However, within the channel (Location D), there is a significant difference in spectral shapes between the linear case and the nonlinear one [Figs. 8(c and g)]. In the nonlinear case, the directional spreading is twice as large as in the linear case. In the linear case, diffraction causes some directional broadening of the spectrum and approximately 3% of the original wave energy enters the channel [estimated from Fig. 9(a)]. However, for the nonlinear case, this is approximately 15% [Fig. 9(b)]. The remarkable difference in variance density spectra between the linear and nonlinear situation points toward the significant effect of nonlinear wave interactions as a mechanism to generate wave energy components that can enter the deeper part.

Directionally Broad-Banded Waves over an Idealized Bathymetry

In the previous section, TRITON and SWAN results were presented for the directionally narrow test case T003 for the idealized geometry. For this geometry, similar computations were carried out for the directionally broad test T004. At the four locations indicated in Fig. 7, 2D variance density spectra have been

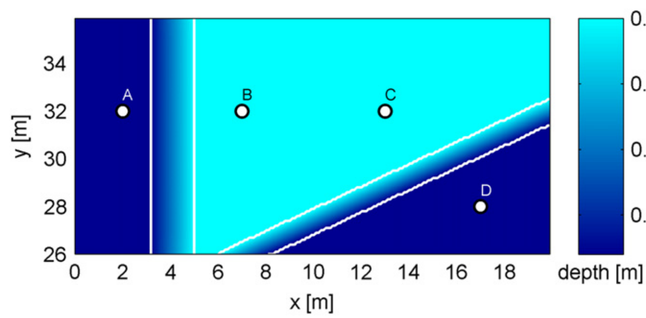

Fig. 7. (Color) Simplified bathymetry with a channel ramp making a 65° angle with the offshore boundary; four output locations have been indicated

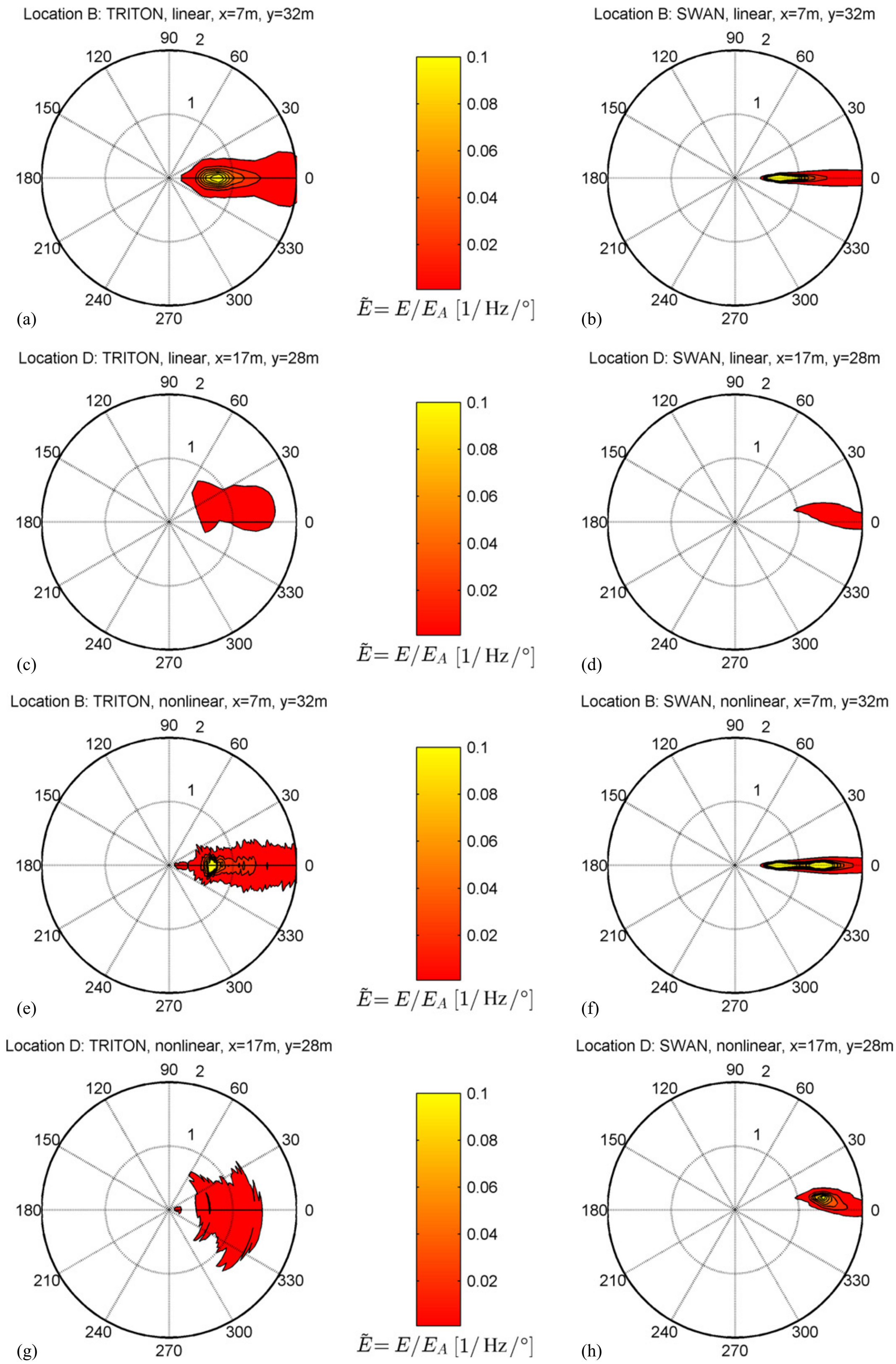

Fig. 8. (Color) Normalized variance density spectra for Test T003, computed by TRITON (a, c, e, g) and SWAN (b, d, f, h) for the idealized bathymetry in Fig. 7 (Cartesian convention); normalized with total variance at Location A; (a–d) reduced wave height $H_{m0} = 0.00082$ m (linear); (e–h) original wave height $H_{m0} = 0.082$ m (nonlinear); (a, b, e, f) shallow location (Location B in Fig. 7); (c, d, g, h) deep location (Location D)

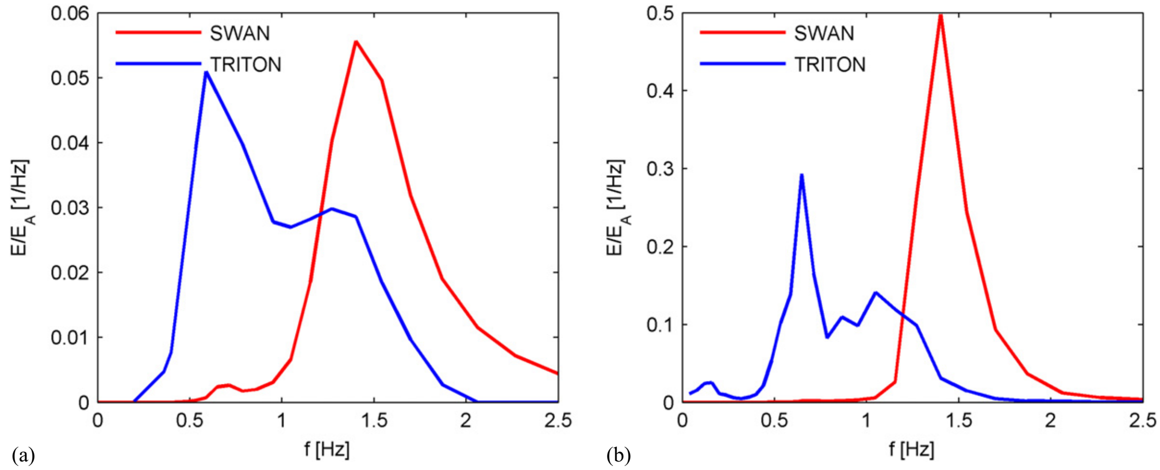

Fig. 9. (Color) Normalized 1D variance density spectra at deep location (Location D) for Test T003, computed by TRITON and SWAN for the idealized bathymetry in Fig. 7; normalized with total variance at Location A; (a) reduced wave height $H_{m0} = 0.00082$ m (linear); (b) original wave height $H_{m0} = 0.082$ m (nonlinear)

presented in Fig. 10; in the left column, the variance density spectra as computed by TRITON have been shown, in the middle column those by SWAN with LTA, and in the right those by SWAN without LTA. The shapes of the TRITON spectra at the first two locations (Locations A and B), i.e., the one in front ($x = 2$ m) and the one behind ($x = 7$ m) the transitional slope, look very similar [compare Figs. 10(a and d)]. Further along the basin at the third location ($x = 13$ m), the variance density spectrum [Fig. 10(g)] shows more directional variation as a results of wave reflection against the channel slope. Compared with TRITON, the transfer of energy to the second harmonic across the transitional slope is much higher for SWAN [see Fig. 10(e)]. The LTA formulation (Eldeberky 1996) in SWAN is a 1D nonlinear self-interaction triad formulation. That means that a wave component only interacts with itself, and via superharmonic interaction energy from the wave component under consideration, it is transferred to its corresponding second harmonic. In addition, it assumes a flat bottom that can approximate only very mild bottom changes. TRITON, however, interacts with all wave components from all directions. According to Toledo (2013), the 2D superharmonic and subharmonic interactions spread the energy over a range of frequencies and directions. The 1D approach in SWAN shows no spreading in directional space and only an increase of the energy of the second harmonic. The effect of the LTA formulation is further illustrated by running SWAN without triad wave interactions. The variance density spectrum hardly changes across the transitional slope [compare Figs. 10(c and f)], whereas the LTA transfers a significant amount of wave energy to the second harmonics [compare Figs. 10(b and e)].

The SWAN spectra at Location C [Figs. 10(h and i)] show an additional peak at the primary frequency of 0.66 Hz at the directions of 40–50°. This is probably caused by the antifocal point at which the channel slope connects to the closed lower side wall. The increase in wave height from this point along the channel can also be observed in SWAN's significant wave height distributions (Fig. 13). The TRITON spectra at Location C [Fig. 10(g)] show a broadening of the spectrum at the peak frequency as well, which may be caused by this antifocal point. Nonetheless, the TRITON spectra are broader at this frequency and have less energy at the second harmonic. As already mentioned, both aspects are the result of the different formulations of nonlinear interactions, 1D superharmonic self-interactions in SWAN versus 2D subharmonic and superharmonic interactions in TRITON. Also, in the deep region at Location D, the 2D spectra computed by TRITON [compare Figs. 10(j and k)] are directionally broader. Therefore, differences appear not only in the shallow region but also in the deep region. This indicates that the nonlinear mechanism in TRITON not only influences the spectral shape in the shallow region, but this better representation of the spectrum in the shallow region also affects the transfer of energy across the channel slope into the deeper part.

Effect of Channel Orientations

In previous tests, the angle between the channel axis and the offshore boundary was 65°. To quantify the influence of the critical angle, the idealized geometry of Fig. 7 (with incoming waves from the left side) is considered. The original channel orientation of 65° with respect to the offshore boundary is applied, as well as orientations of 30°, 50°, and 75°. The mean wave direction is still 90° with respect to the offshore boundary. For the conditions of Test T004 ($T_p = 1.45$ s), spatial distributions of the significant wave height, as well as the SWAN-computed and TRITON-computed 2D variance density spectra at Locations B and D (shallow and deep), are presented in Figs. 11–13 for each of the channel orientations 30°, 50°, and 65°. Because the spatial distributions of the significant wave height for the channel orientations of 65° and 75° are almost similar, the latter is not shown here. In these figures, the geometries are sketched by the contour lines of 0.20 m (shallow) and 0.38 m (deep) water depth. According to Snell's law, the critical channel orientation is 50°, above which wave components propagating under an angle of 0° will not be able to enter the deep part.

For the 30° channel orientation, most of the energy propagates into the deep part (Fig. 11), whereas for channel orientations around (Fig. 12) and above (Fig. 13) the critical angle, the wave height reduces strongly at the channel slope. The reduction in significant wave heights at deep water is slightly smaller for the TRITON results than for the SWAN results [compare Figs. 11 (a and d)]. Furthermore, the geometric optics approximation in SWAN causes the wave energy to spread out over the shallow region in front of the channel. The sharper the angle between the channel axis and the mean wave direction, the larger this area is. This is also observed in the TRITON computations. The TRITON results also show reflections against the closed walls, especially near the upward transition slopes towards the shallow flat (red parts on upper and lower part of the panels).

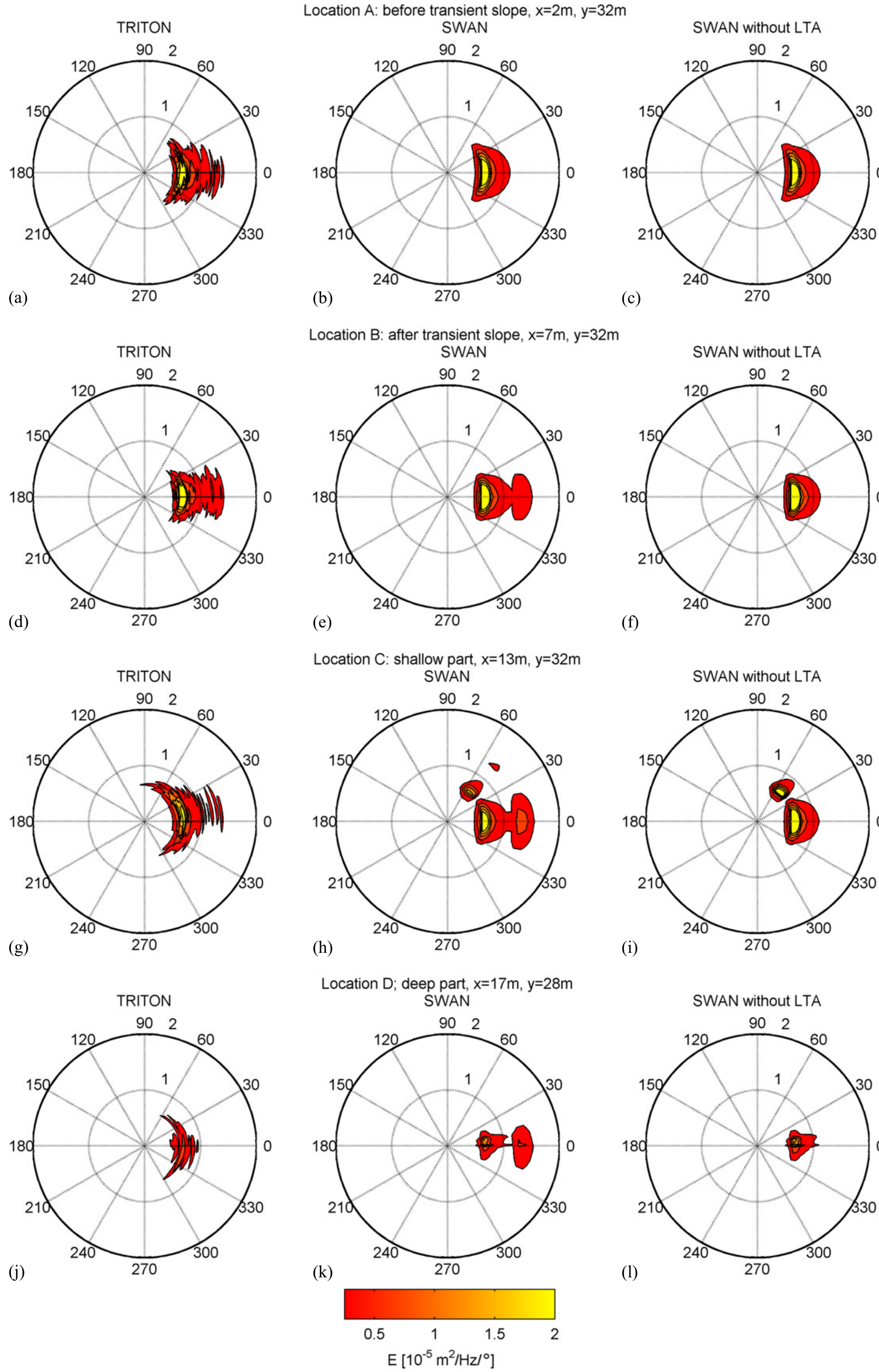

Fig. 10. (Color) Variance density spectra for Test T004 ($H_{m0} = 0.082$ m, $T_p = 1.45$ s, Dir.spr. = 20°), computed by TRITON (a, d, g, j), SWAN (b, e, h, k), and SWAN without its 1D LTA nonlinear transfer mechanism (c, f, i, l) at the four locations in Fig. 7 (Cartesian convention)

J. Waterway, Port, Coastal, Ocean Eng.

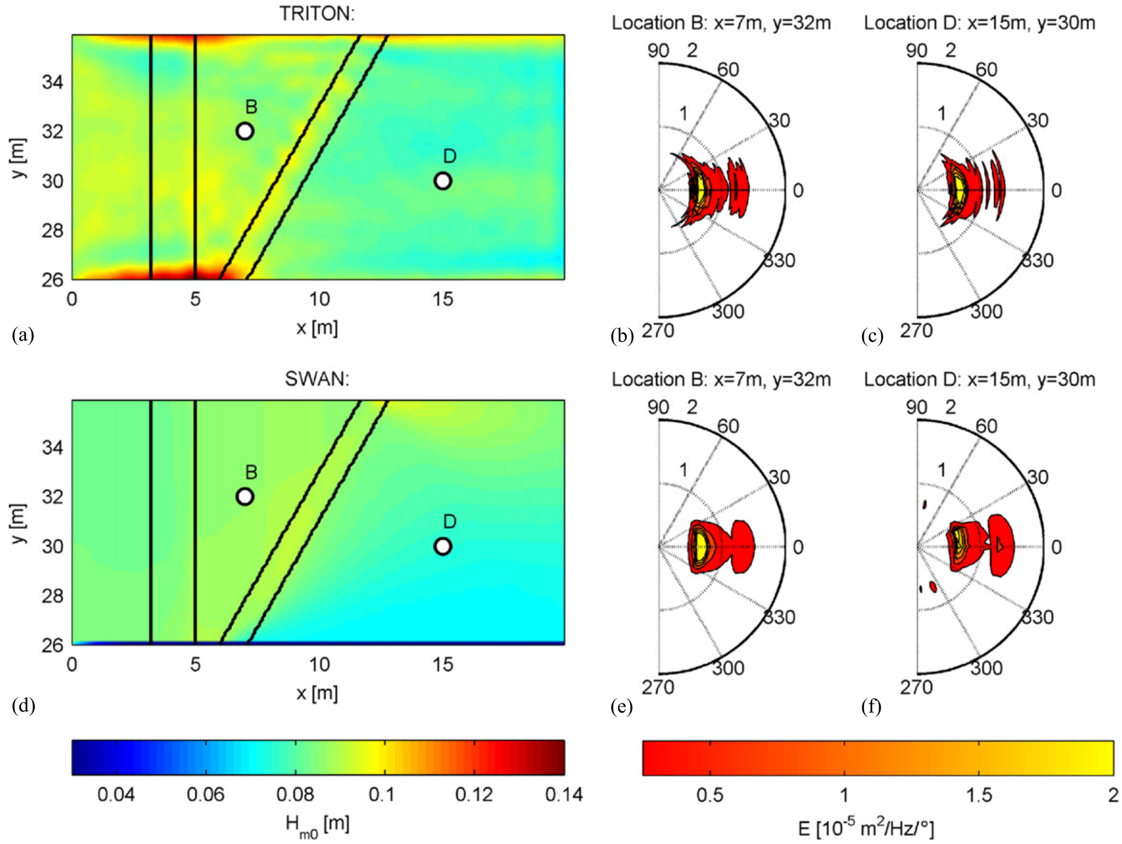

Fig. 11. (Color) Spatial distribution of significant wave height and 2D energy density spectra at two output locations, computed by TRITON (a, b, and c) and SWAN (d, e, and f), for Test T004 for the 30° channel orientation

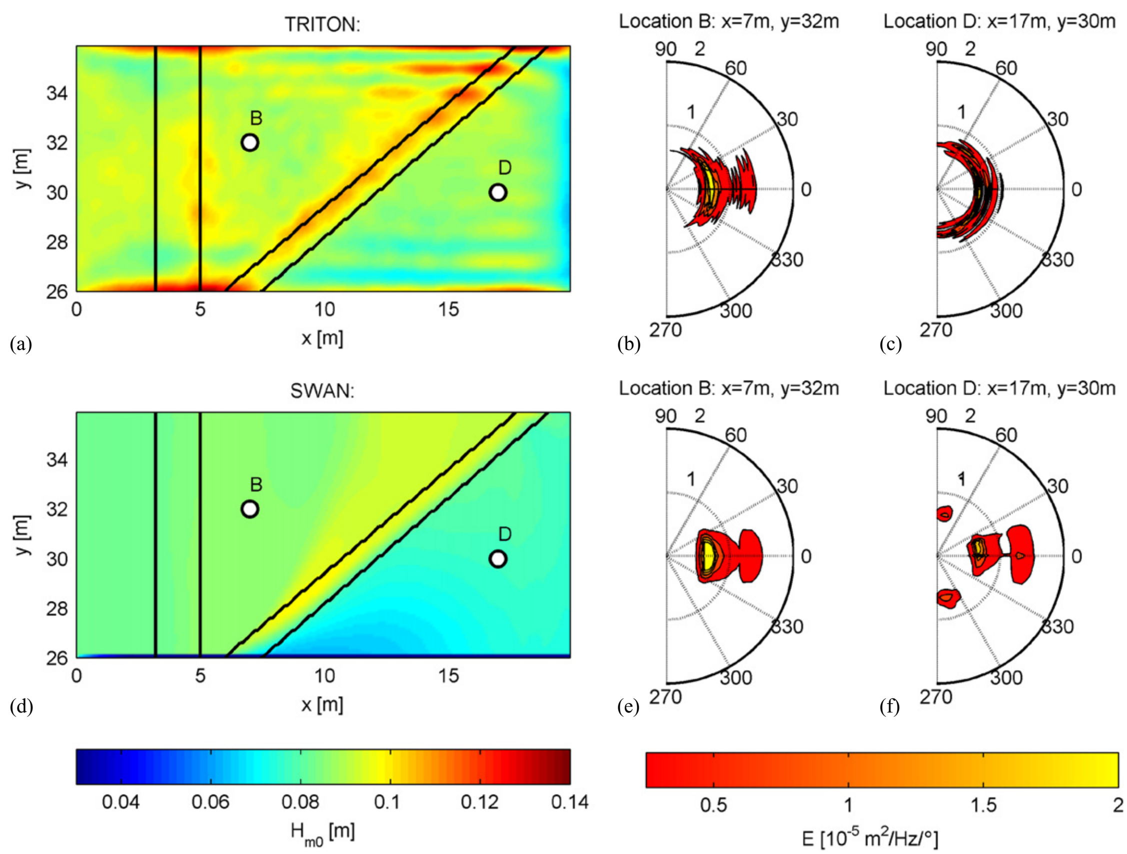

Fig. 12. (Color) Spatial distribution of significant wave height and 2D energy density spectra at two output locations, computed by TRITON (a, b, and c) and SWAN (d, e, and f) for Test T004 for the 50° channel orientation

Whereas the significant wave height change computed by SWAN and TRITON is comparable in a qualitative sense, this is clearly not valid for the 2D energy density spectra. For the 30° channel orientation, the energy distributions of SWAN and TRITON over the directions, as well as over the frequencies, still show strong similarities; see Figs. 11(b and e). Across the channel slope, refraction slightly modifies the propagation angle in both SWAN and TRITON [see Figs. 11(c and f)]. For the channel orientation of 50° and higher, the energy in the deeper part is reduced. At the primary peak of the SWAN spectra, the energy content and direction are modified by refraction [compare Figs. 12(e and f)]. The second harmonics in SWAN are hardly affected by the channel. These shorter waves feel the bottom to a lesser extent. As was already observed in previous sections, the amount of energy of the second harmonics in TRITON is smaller than predicted by SWAN in the shallow region [compare Figs. 12(b and e)]. Consequently, this is also the case in the deeper region downwave of the channel slope. However, owing to 2D nonlinear subharmonic and superharmonic interactions on TRITON, the directional spreading at the primary peak increases on the shallow part. More wave components approach the channel under such an angle that they are not hampered by refraction when entering the deep region. Furthermore, the nonlinear interactions broaden the directional range of the spectrum on the downward slope. Clearly, the variance density spectra computed by TRITON are broader in directional space than those computed by SWAN.

Evaluation of Academic Test Results

As already mentioned, the nonlinear triad interaction formulation (LTA) in SWAN is a 1D colinear approach. For long-crested waves, the difference in nonlinear behavior between SWAN and TRITON may therefore be smaller. In Fig. 8, the variance density spectra for the directionally narrow-banded Test T003 were presented. Comparing the 2D spectra for Test T003 and its linear variant shows that the variance densities at the deeper location computed by SWAN are similar in both situations. Apparently nonlinear interactions in SWAN are not effective over the slope of the channel. However, this is not true for TRITON. Because of diffraction, energy at the primary peak is present at the deeper location in both the linear and nonlinear case, but the directional spreading is twice as large for the nonlinear case. As for the test with directional spreading, the directional changes in the primary harmonic due to 2D nonlinear interactions result in smaller attack angles that increase the wave energy transfer for narrow-spread seas to the deeper region. The SWAN model's 1D nonlinear triad interaction formulation lacks the capability of changing the propagation direction of wave energy and hence fails to predict this phenomenon. Deliberately, the term *narrow-spread seas* is used instead of long-crested waves because the wave field on the flat region is no longer long-crested but contains a limited amount of directional spreading. Okihiro et al. (1992) and Herbers et al. (1994) concluded that for upslope conditions, directional spreading reduces the nonlinear interactions between primary components. From comparing the 2D spectra, one cannot confirm this conclusion because refraction is a dominant mechanism next to 2D nonlinear wave interactions.

Overall, it can be concluded that owing to refraction at the channel slope, the wave transmission into and across the channel reduces significantly when the wave attack angle with respect to the channel axis decreases. The 2D superharmonic and subharmonic

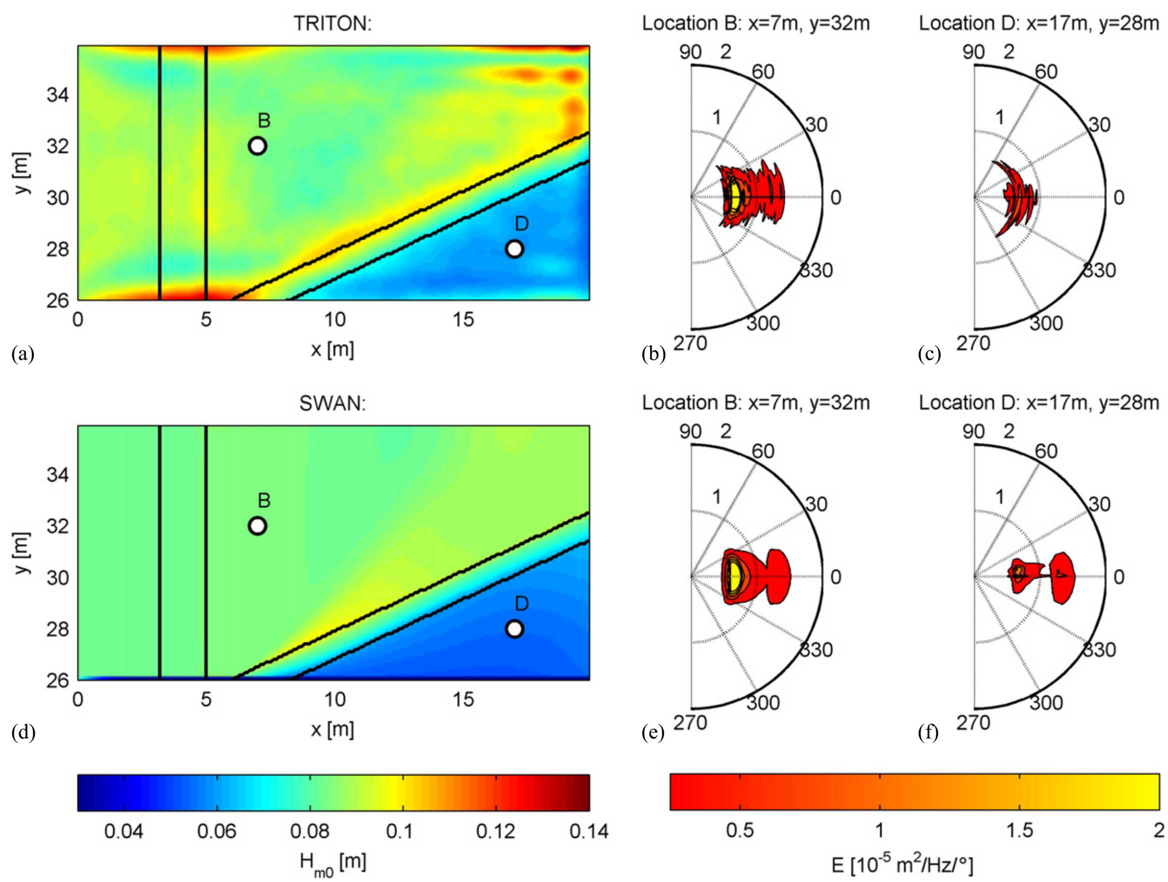

Fig. 13. (Color) Spatial distribution of significant wave height and 2D energy density spectra at two output locations, computed by TRITON (a, b, and c) and SWAN (d, e, and f) for Test T004 for the 65° channel orientation

interactions in TRITON spread the energy over a range of frequencies and directions. This mechanism is not present in SWAN. The directional broadening of the variance density spectra allows more wave energy to enter the channel. This results in an underprediction of the transmitted wave energy by SWAN compared with TRITON and reality.

Towards Practical Situations

In previous sections, wave propagation over idealized geometries was considered as a strong simplification for the purpose of grasping SWAN's behavior in a complex bathymetry such as the Wadden Sea. The omission of the 2D nonlinear interactions in SWAN was held responsible for a significant part of SWAN's underprediction of swell-wave energy penetration into and across channels. The question of what role this mechanism plays in calculations of the complex Wadden Sea is currently hard to answer because directional measurements in this area are scarce.

Nevertheless, one can indicate the effect of the Wadden Sea channels and make deductions about the accuracy of swell-wave propagation in SWAN's calculation. For this purpose, a hindcast of the storm of December 5–6, 2013, was carried out. The model settings are similar to the ones mentioned in the section "Laboratory Channel Experiments." Because the results are discussed only qualitatively, no additional details about the model settings have been given. For the illustration presented here, the conditions at 1200 hours Central European Time (CET) on December 6, 2013 are considered. The tidal phase was high water slack, so the current speed is low. The wind speed was 20 m/s from direction 300°N. An offshore significant wave height of 7 m and peak period of 12.3 s were observed for this time instant.

The Eastern Wadden Sea contains a main navigation channel and many smaller channels, as is illustrated in Fig. 14(a). The figure depicts the area just east of the island of Borkum (white box). Four locations have been considered, two in the channel (Locations 3 and 4), one in the shallow area between two channels (Location 1), and one on the main channel edge (Location 2). The energy density spectra computed by SWAN at these four locations have been given in Figs. 14(c–f). The wave energy at the channel locations propagates along the channel, more or less in the wind direction. At the channel edge, the waves refract while propagating from deep to shallow water depths, explaining the wave energy from the north at Location 2 [Fig. 14(d)]. At Location 1, which is further away from the channel edge, energy from the north can also be observed [Fig. 14(c)]. However, this location is dominated by energy from the west, probably because of refraction from the channel on the left of the main channel. This western component can also be observed at Location 2. However, the energy density spectra at Locations 3 and 4 [Figs. 14(e and f)] indicate that this energy does not reach the deeper channel. This means that part of the computed wave energy propagates towards the channel but does not enter the channel.

This behavior is comparable to the observations in the idealized cases. Refraction is responsible for the piling-up of energy at the channel edge and on the channel's shallow parts. Although not confirmed with TRITON results owing to the high computational effort required for such a large domain, it is most likely that the conclusion about the omission of 2D nonlinear interactions in SWAN also holds for more practical situations such as in the Wadden Sea.

The accumulation of energy at channel edges and at locally shallow parts inside the channel indicates that downwave of this region SWAN results should be treated with care. The significance of SWAN's inaccuracies, as of any other wave-action model, due to incorrect modeling of the triad nonlinear wave interactions, will depend on various parameters, such as the shape of the channels in the coastal region, the attack angle of the incident waves, the spectral shape, and because this paper discusses a nonlinear phenomenon, of course, the wave steepness. Therefore, one cannot provide a generic evaluation of the error's magnitude. In practical situations, the wave evolution in this downwave region will also be affected by other, partly unaccounted-for physical mechanisms or input inaccuracies (e.g., the effects of currents and current shear on the waves, inaccuracies in the bathymetry map, inaccuracies in the local wind input, etc.). Compared with these possible sources of uncertainties, the effect of incorrect modeling of the nonlinear interactions at the channel region may be of less importance. Nevertheless, nonlinear interactions have unique influence on the spectral shape, which might be low in magnitude but of high importance in its influence on sediment transport or harbor agitation, for example. Observing trapped wave energy on the channel edge implies that some of this energy should have crossed the channel's edge. The amount of trapped energy gives an indication of the error's magnitude. As mentioned previously, no generic estimate can be given. Therefore, it is recommended that engineers treat the possibly incorrect SWAN results downwave of the channel with care. Unfortunately, until an appropriate 2D source term for triad nonlinear wave interactions is available, the problem can only be mitigated using the diagnostic modeling measures mentioned in the first section, such as limiting the refraction of swell waves and decreasing bottom friction.

Conclusions and Recommendations

Comparison with field measurements in the Wadden Sea during severe storms showed that the phase-averaged wave model SWAN underpredicts the wave penetration into this complex tidal inlet system. On the basis of laboratory measurements and successive numerical computations with SWAN and the Boussinesq-type wave model TRITON, the hypothesis was raised that 2D nonlinear interactions are an important mechanism that changes the energy density spectrum in such a way that additional wave energy is transmitted into and across channels. Whenever these nonlinear interactions are not modeled accurately, an unrealistic amount of energy is trapped on the channel slopes owing to wave refraction, at which point waves attack channels under an angle.

Using a linear approximation, the primary wave components are not able to enter the channel when the angle of attack is larger than the frequency-dependent critical angle owing to refraction. Using the research by Toledo (2013), it is concluded that 2D subharmonic and superharmonic nonlinear interactions broaden the variance density spectrum not only in frequency space but also in directional space, both in upslope and downslope situations. Thus, in the situation where oblique waves approach a channel, nonlinear interactions in the shallow part as well as those initiated by the change in bathymetry at the channel edge ensure that more energy is present at angles smaller than the critical angle and therefore more wave energy propagates into and across the channel than if the linear approximation is used.

As was already concluded by Magne et al. (2007), the wave attack angle to the channel is important. In this work, it is observed that both in the SWAN and TRITON computations, the wave energy at the primary peak of the spectrum reduces significantly when the wave attack angle with respect to the channel axis decreases. The 2D subharmonic and superharmonic interactions in TRITON spread the energy over a range of frequencies and directions. This affects the wave energy transfer to the deeper

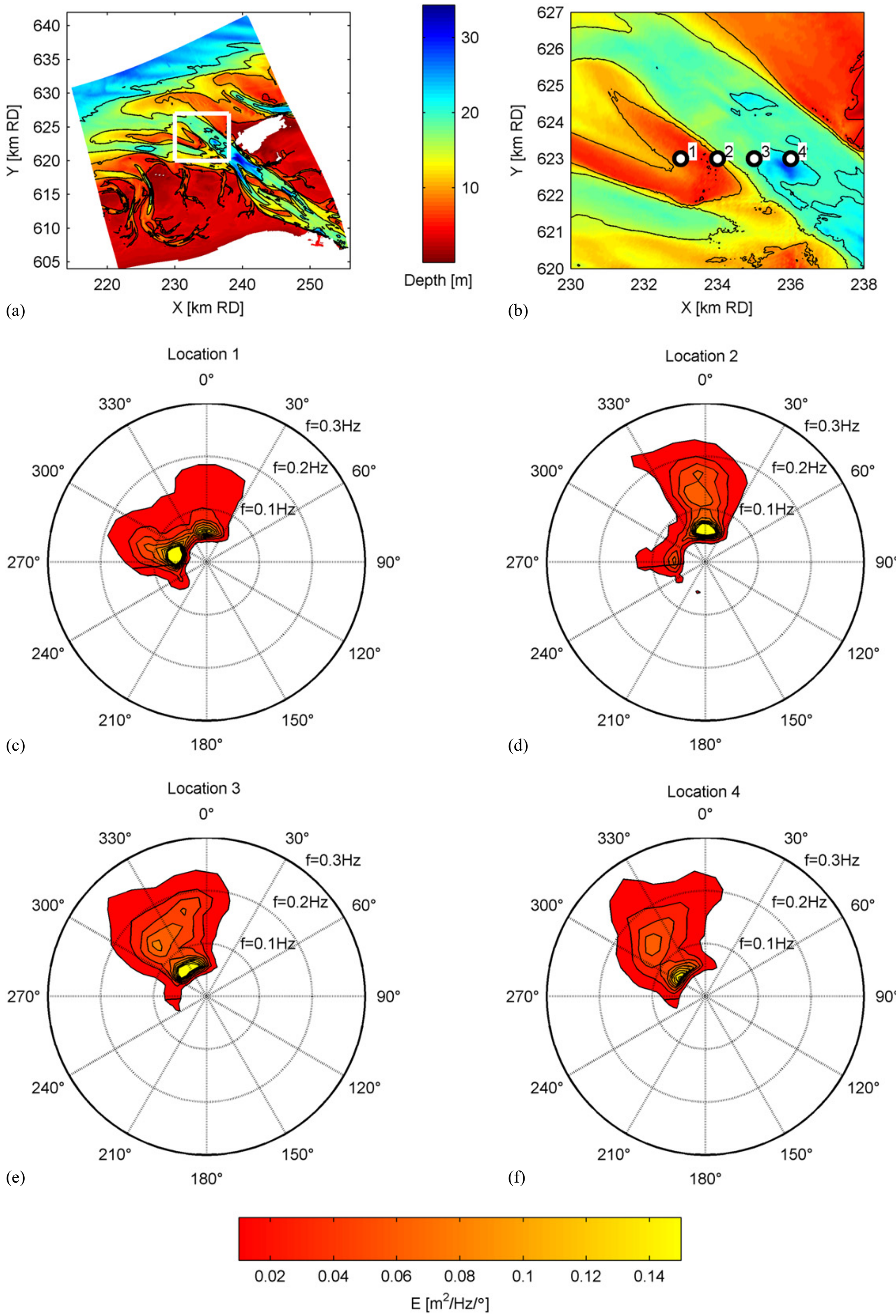

Fig. 14. (Color) Two-dimensional variance density spectra at four locations in the Eastern Wadden Sea (Netherlands), as computed by SWAN (nautical convention). The storm instant considered is December 6, 2013 at 1200 hours (CET). The water depth at this instant is shown in (a). The area in (b) denotes the area in the white box in (a). The black lines indicate depth contours at 5, 10, 15, and 20 m. The four locations are indicated with white dots

region across the channel slope. For both directionally broad spread seas and for directionally narrow spread seas, the 2D subharmonic and superharmonic interactions are effective and change the spectral distribution of energy over frequencies and, very relevant for the present scope, over directions. However, SWAN's 1D nonlinear self-interaction triad formulation (LTA) does not include a mechanism to redistribute the energy over a wider range of directions. Absence of this spectrum-broadening mechanism leads to an underestimation of the wave propagation into and across the channel.

The hypothesis that 2D nonlinear interactions, especially the subharmonic interactions, provide a mechanism to transmit energy from flats into the channel is confirmed using the analysis performed here. Because this type of nonlinear wave interaction has not been implemented in SWAN (or any other wave-action equation model), this study has found an explanation for the underprediction by SWAN of wave-energy penetration into and across channels.

The conclusion is particularly valid for wave propagation over relatively simple geometries as waves approach channels near harbor entrances. Understanding that the wave spectrum broadens in the directional space, when waves propagate on the slopes of an approach channel towards the harbor entrance, may lead to adaptations in the design of approach channels, as possibly more swell-wave energy from unexpected directions reaches the harbor. As a consequence, harbor oscillations and high forces on moored ships can be prevented. In addition, the wave loading on breakwaters near harbor entrances can be either too high or too low if the wave propagation across approach channels is not accurately accounted for.

Although not confirmed with measurements or TRITON results, it is most likely that the conclusion about the omission of 2D nonlinear interactions in SWAN also holds for more complex geometries such as the Wadden Sea. Accumulation of wave energy at channel edges and at locally shallow parts inside the channel is an indicator of possibly wrong SWAN results. These results, and those downwave of this region, should be treated with care.

Owing to the size of the computational domain, which consists of dozens of wave lengths, a phase-averaged model such as SWAN is applied to determine the wave conditions in coastal systems with complex bathymetries such as tidal inlet systems or approach channels for harbors. A phase-resolving model such as TRITON cannot replace SWAN for these applications. Essential wave physics, e.g., wind input, is lacking in a phase-resolving model such as TRITON, and the computational time for all computations would be too large. Therefore, it is recommended that an alternative be developed for the presently implemented 1D three-wave interaction formulation in SWAN such that the broadening of the directional range can be accurately modeled.

Currently, stochastic (phase-averaged) wave-action equation (WAE) models, such as the SWAN model, do not hold an adequate formulation that accounts for 2D triad interactions. The 1D formulations, which have already been coded for WAE models, include the LTA formulation (Eldeberky and Battjes 1995) and consist of a partial description of the phenomenon, including only superharmonic self-interactions and a flat-bottom assumption. The stochastic parametric model (SPB) model (Becq-Girard et al. 1999) advanced the description by including all possible interactions, both superharmonic and subharmonic, but limited the formulation for very small changes in the bispectra as the waves shoal. Stiassnie and Drimer (2006) and Toledo and Agnon (2012) presented a 1D formulation that accounts for bottom changes and both subharmonic and superharmonic interactions. These formulations were not yet implemented in WAE models. A 2D formulation was given by Eldeberky (1996) with a flat-bottom assumption but was never implemented. Janssen (2009) derived and implemented a 2D formulation in the WAM model, again with a flat-bottom assumption. Such 2D formulations are essential for extending the applicability of WAE models in the near-shore region. Nevertheless, their inherent flat-bottom assumptions are expected to limit the validity of these formulations to very mild sloping beaches with no channels or any other complex bathymetry. A 2D formulation that relaxes the flat-bottom assumption is yet to be derived.

Acknowledgments

Support from the Legal Assessment Instruments WTI2017 project, commissioned by National Water Authority Rijkswaterstaat in the Netherlands, is kindly appreciated. Mr. Daniel Dusseljee and Mr. Stephan van der Biezen (Witteveen+Bos) are acknowledged for their interest and discussions on wave propagation in relation to approach channels.

References

Alam, M. R., Liu, Y., and Yue, D. K. P. (2010). "Oblique sub- and superharmonic bragg resonance of surface waves by bottom ripples." *J. Fluid Mech.*, 643, 437–447.

Alkyon. (2009). "Analysis of wave penetration into the eastern Wadden Sea." *Alkyon Rep. No. A2302*, Alkyon Hydraulics, Marknesse, Netherlands.

Becq-Girard, F., Forget, P., and Benoit, M. (1999). "Non-linear propagation of unidirectional wave fields over varying topography." *Coastal Eng.*, 38(2), 91–113.

Benoit, M., Frigaard, P., and Schäffer, H. A. (1997). "Analysing multidirectional wave spectra: A tentative classification of available methods." *Proc., IAHR Seminar Multidirectional Waves and Their Interaction with Structures, 27th IAHR Congr.*, San Francisco, 131–158.

Booij, N., Ris, R. C., and Holthuijsen, L. H. (1999). "A third generation wave model for coastal regions: 1. Model description and validation." *J. Geophys. Res.*, 104(C4), 7649–7666.

Borsboom, M. J. A., Doorn, N., Groeneweg, J., and van Gent, M. R. A. (2000). "A Boussinesq-type model that conserves both mass and momentum." *Proc., 27th Int. Conf. on Coastal Eng.*, ASCE, Sydney, NSW, Australia, 148–161.

Deltares/Alkyon (2009). "Wave propagation through tidal inlet systems." *Deltares Rep. No. 1200114-002-HYE-0006*, Deltares Delft, Netherlands.

Dusseljee, D., Kuiper, C., and Klopman, G. (2012). "Wave modeling in navigation channels." *Proc., Coastlab 2012 Conf.*, IAHR, Ghent, Belgium, 465–474.

Eldeberky, Y. (1996). "Nonlinear transformations of wave spectra in the nearshore zone." Ph.D. thesis, Delft Univ. of Technology, Delft, Netherlands.

Eldeberky, Y., and Battjes, J. A. (1995). "Parametrization of triad interaction in wave energy models." *Proc., Coastal Dynamics Conf.*, ASCE, Gdansk, Poland, 140–148.

Eslami S. A., van Dongeren, A., and Wellens, P. (2012). "Studying the effect of linear refraction on low-frequency wave propagation (physical and numerical study)." *Proc., 33rd Int. Conf. on Coastal Engineering*, CERC, Santander, Spain.

Groeneweg, J., Doorn, N., Borsboom, M. J. A., and van Gent, M. R. A. (2002). "Boussinesq-type modeling of measured wave breaking on a circular shoal." *Proc., 28th Int. Conf. on Coastal Engineering*, World Scientific, Cardiff, U.K., 495–507.

Hasselmann, K., et al. (1973), "Measurement of windwave growth and swell decay during the Joint North Sea Wave Project (JONSWAP)." *Dtsch. Hydrogr. Z.*, A8(12), 95.

Herbers, T. H. C., Elgar, S. and Guza, R. T. (1994). "Infragravity-frequency (0.005-0.05 Hz) motions on the shelf. Part I: Forced waves." *J. Phys. Oceanogr.*, 24(5), 917–927.

Holthuijsen, L. H., Herman, A., and Booij, N. (2003). "Phase-decoupled refraction-diffraction for spectral wave models." *Coastal Eng.*, 49(4), 291–305.

Janssen, P. A. E. M. (2009). "On some consequences of the canonical transformation in the Hamiltonian theory of water waves." *J. Fluid Mech.*, 637, 1–44.

Kim, T., Lin, L.-H., and Wang, H. (1994). "Application of maximum entropy method to the real sea data." *Proc., 24th Int. Conf. on Coastal Engineering*, ASCE, Kobe, Japan, 340–355.

Kobune, K., and Hashimoto, N. (1986). "Estimation of directional spectra from the maximum entropy principle." *Proc., 5th Int. Offshore Mechanics and Arctic Engineering (OMAE) Symp.*, ASME, Tokyo, 80–85.

Liu, Y., and Yue, D. K. P (1998). "On generalized bragg scattering of surface waves by bottom ripples." *J. Fluid Mech.*, 356, 297–326.

Magne, R., Belibassakis, K. A., Herbers, T. H. C., Ardhuin, F., O'Reilly, W. C., and Rey, V. (2007). "Evolution of surface gravity waves over a submarine canyon." *J. Geophys. Res.*, 112(C1), C01002.

Okihiro, M., Guza, R. T., and Seymour, R. J. (1992). "Bound infragravity waves." *J. Geophys. Res.*, 97(C7), 11453–11469.

Stiassnie, M., and Drimer, N. (2006). "Prediction of long forcing waves for harbor agitation studies." *J. Waterway, Port, Coastal, Ocean Eng.*, 10.1061/(ASCE)0733-950X(2006)132:3(166), 166–171.

Toledo, Y. (2013). "The oblique parabolic equation model for linear and nonlinear wave shoaling." *J. Fluid Mech.*, 715, 103–133.

Toledo, Y., and Agnon, Y. (2009). "Nonlinear refraction–diffraction of water waves: The complementary mild-slope equations." *J. Fluid Mech.*, 641, 509–520.

Toledo, Y., and Agnon, Y. (2012). "Stochastic evolution equations with localized nonlinear shoaling coefficients." *Eur. J. Mech. B. Fluids*, 34, 13–18.

Van der Westhuysen, A. J. (2009). "Modeling of depth-induced wave breaking over sloping and horizontal beds." *11th Int. Workshop on Wave Hindcasting and Forecasting*, Environ. Can., Halifax, NS, Canada, ⟨http://www.waveworkshop.org/11thWaves⟩ (Oct. 18–23, 2009).

Van der Westhuysen, A. J. (2010). "Modeling of depth-induced wave breaking under finite depth wave growth conditions." *J. Geophys. Res.*, 115(C1), 1–19.

Van der Westhuysen, A. J., et al. (2012). "Improvements in spectral wave modeling in tidal inlet seas." *J. Geophys. Res.*, 117(C11), 1–23.

Zijlema, M., and van der Westhuysen, A. J. (2005). "On convergence behavior and numerical accuracy in stationary SWAN simulations of nearshore wind wave spectra." *Coastal Eng.*, 52(3), 237–256.

Zijlema, M., van Vledder, G. P., and Holthuijsen, L. H. (2012). "Bottom friction and wind drag for wave models." *Coastal Eng.*, 65, 19–26.